Strong cavity-pseudospin coupling in monolayer transition metal dichalcogenides

Amrit De* and Roger K. Lake†

Department of Electrical and Computer Engineering, University of California, Riverside, California 92521, USA

(Received 5 January 2016; revised manuscript received 26 April 2017; published 25 July 2017)

Strong coupling between the electronic states of monolayer transition metal dichalcogenides (TMDCs) such as MoS_2, $MoSe_2$, WS_2, or WSe_2, and a single in-plane optical cavity mode gives rise to valley- and spin-dependent cavity-QED effects. The Dirac Hamiltonian for this two-dimensional gapped semiconductor with large spin-orbit coupling facilitates pure Jaynes-Cummings-type coupling with spin-valley locking—providing an additional handle for spintronics using circularly polarized light. Besides being an on-chip light source, the strong cavity coupling causes the TMDC monolayer to act as a spontaneous spin oscillator. In addition, this system can be a sensitive magnetic field sensor for an in-plane magnetic field. It also displays unusual persistent Rabi oscillations between different conduction-band states that are insensitive to small magnetic field variations. Our analysis for dissipation due to finite exciton relaxation times and cavity losses suggests that these effects are observable.

DOI: 10.1103/PhysRevB.96.035436

I. INTRODUCTION

Light and matter can become strongly coupled in an optical cavity giving rise to qualitatively new physics and resulting in numerous applications in laser physics, optoelectronics, and quantum information processing. The coherent coupling of light and matter in such systems is described by cavity quantum electrodynamics (QED). The advent of quantum information processing has led to significant activity investigating optical cavity-like systems for coherent conversion of qubits between matter or topological states to phonons, photons, and circuit oscillators [1–9]. Strong cavity coupling allows solid-state qubits to communicate via the photons [10] or can even allow photonic qubits to interact via the atom [11].

The atom-photon coupling should be very strong in two dimensions because of the small mode volume. Monolayers and bilayers of transition metal dicalcogenides (TMDCs) are gapped two-dimensional (2D) Dirac materials with strong spin-orbit (SO) interactions. The quantum Hall effect is yet to be observed in these materials. Meanwhile it has been shown that they have excellent optical properties. TMDCs strongly couple to light since they have direct band gaps and their large effective masses result in a large density of states and excitonic binding energies [12–14]. Furthermore, TMDC's large SO coupling results in spin-valley polarized valence bands [15,16]. The magnetic moment associated with their valley pseudospin gives rise to valley-dependent circular dichroism [13,14]. In general, the polarization-dependent photoluminescence for WSe_2 indicates that the optical selection rules derived from the single-particle picture are also inherited by neutral and charged excitons [12].

Access to these valley and spin degrees of freedom can allow for hybrid on-chip optoelectronic and spintronic devices. Since the spin degrees of freedom for a band are coupled to a particular valley in momentum space, TMDCs might also be candidates for qubits with long coherence times, and there have been suggestions for implementing single-qubit gates in TMDC quantum dots [17] and bilayers [18].

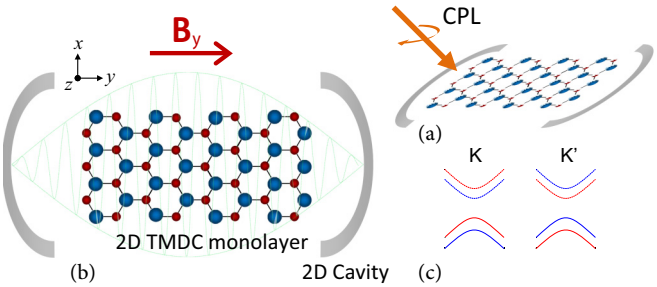

FIG. 1. Schematic of a monolayer TMDC in a 2D photonic cavity (a) with incident circularly polarized light (CPL) to break the valley degeneracy and (b) with an in-plane magnetic field B_y, for magnetometry. (c) Band structure about K and K' showing lifting of conduction-band degeneracy from B_y. Colors indicate the band's spin.

There are a number of ways in which 2D materials can strongly couple to various cavity modes. Graphene-TMDC heterostructures are used for photovoltaics [19] and graphene (Gr) can couple to a photonic crystal's evanescent mode [20]. There have also been suggestions for coupling quantum two-level systems (TLSs) to surface plasmon modes in Gr [21]. Very recently, 2D exciton lasers [22] have been experimentally realized by placing TMDCs inside microdisks [23], tunable Bragg reflectors [24], and on photonic crystals [25]. These are often geared toward lasers and photovoltaics and the coupling to the electromagntic mode in the cavity is different [22–25] from what we are interested in.

We go beyond traditional optoelectronics in this paper. Unusual properties and device functionalities are shown to arise from strong light-matter interactions between a gapped valley-selectable SO-split 2D Dirac material and a single in-plane optical cavity mode. Usually the TLS-field coupling occurs via a dipole- or nonlinear-interaction-type terms in cavity QED. Here, canonically transforming the linear k-dependent 2D Dirac term, directly gives Rabi- or Jaynes-Cummings coupling between the cavity mode and the lattice pseudospin. This leads to interesting effects since the valley and spin indices are coupled in TMDCs, and each valley can

*amritde@gmail.com
†rlake@ece.ucr.edu

be addressed by using circularly polarized light (CPL) of a given handedness [26].

In a suitable optical cavity this could lead to spontaneous spin oscillations for spintronics. However, CPL flips its handedness upon reflection from a conventional surface—hence it is not easy to design a cavity that will only sustain either just left or right CPL. Some reflective chiral surfaces can suppress this cross polarization [27,28]. Alternatively, the evanescent mode of a chiral photonic crystal [29] could also be used, but then the TLS-cavity coupling will not be too strong.

We suggest a different approach and point out an additional advantage of a fully 2D architecture. 2D resonator cavities are now quite common in circuit QED [8,9]. In the strongly coupled system of a 2D TMDC monolayer inside a 2D cavity, spontaneous vacuum Rabi oscillations occur even in the absence of photons. Since a 2D cavity only supports linearly polarized electromagnetic modes, Rabi oscillations occur for both valleys with opposite spin. We propose introducing an additional CPL beam incident on the 2D cavity-QED system [see Fig. 1(a)]. Sufficiently intense CPL selects valley. Since intravalley transitions conserve spin, this leads to spin-polarized Rabi flopping. These spin oscillations can occur spontaneously with zero cavity photons. The overall degree of valley polarization depends on the CPL's intensity which blue-shifts the Rabi frequency. At higher photon number coherent cavity states, *spin-polarized* collapse and revival of Rabi oscillations occur.

This cavity-pseudospin system also has other applications. It is a highly sensitive sensor of an in-plane magnetic field. An in-plane magnetic field shifts the vacuum Rabi frequency. We show that this frequency shift is scale invariant, which is a very promising finding. Whereas one usually seeks strong cavity-TLS coupling, here the scale invariance suggests high field sensitivity for weak cavity coupling. This can lead to important field sensor applications.

In addition, this 2D system without any of the additional fields can also be an on-chip coherent light source and a frequency comb. We explicitly calculate dissipation from cavity losses and TMDC's exitonic lifetimes and show that the effects discussed in this paper will be observable.

II. THE MODEL

Consider the model Hamiltonian for a monolayer TMDC in an in-plane magnetic field along y: $H_o' = H_o + H_b$, where H_o is the following effective 4×4 two-band $\mathbf{k}\cdot\mathbf{p}$ Hamiltonian for a given valley,

$$H_o = u(\tau\tilde{\sigma}_x k_x + \tilde{\sigma}_y k_y) + \frac{E_g}{2}\tilde{\sigma}_z + \frac{\Delta_{so}}{2}\tau s_z(\tilde{\sigma}_z - I), \quad (1)$$

where E_g is the band gap, Δ_{so} is the SO splitting, and u is the velocity. Here $H_b = g_\parallel \mu_B B_y s_y$ where $g_\parallel$ is the in-plane g factor and μ_B is the Bohr magneton. In this paper we work in normalized units of $g_\parallel B_y$, because published $g_\parallel$ data is presently sparse.

The Pauli spin matrices along j are s_j, and $\tilde{\sigma}_j$ are the pseudospin Pauli matrices in the orbital basis, $\{\psi_c,\psi_v^\tau\} = \{|d_{z^2}\rangle, |d_{x^2+y^2} + i\tau d_{xy}\rangle\}$. It is implied that $\tilde{\sigma}_j = I\otimes\sigma_j$ and $s_j = \sigma_j \otimes I$.

TABLE I. Coupling strengths; $\Lambda_\pm$ corresponds to $\omega_\pm = E_g \pm \Delta_{so}$ transitions for various TMDCs.

Material	Λ_- (GHz)	Λ_+ (GHz)
MoS_2	140	144
WS_2	200	247
$MoSe_2$	118	124
WSe_2	148	165

First consider the case of a monolayer TMDC in a cavity with $B_y = 0$. For a reflective cavity, with the single mode of an electric field oscillating along $\hat{x}$, one can canonically transform $k_x \to k_x + A_x$, where A_x is the vector potential along x. The TMDC-cavity coupling Hamiltonian is $H_i = u\tau\tilde{\sigma}_x A_x(t) = \Lambda\tau\tilde{\sigma}_x(a^* e^{i\omega t} + a e^{-i\omega t})$ where Λ is the coupling constant between the cavity's electric field and the TMDC bands. Second quantizing the cavity field and invoking the rotating wave approximation, $\Lambda\tau\tilde{\sigma}_x(a^\dagger + a) \approx \Lambda\tau(a^\dagger\tilde{\sigma}_- + a\tilde{\sigma}_+)$, where $\sigma_\pm = \sigma_x \pm i\sigma_y$, and $a^\dagger(a)$ are the photon creation (annihilation) operators, the total system Hamiltonian [see Fig. 1(b)] can be expressed as

$$H = u(\tau\tilde{\sigma}_x k_x + \tilde{\sigma}_y k_y) + \frac{E_g}{2}\tilde{\sigma}_z + \frac{\Delta_{so}}{2}\tau s_z(\sigma_z - I) + \frac{\omega}{2}a^\dagger a + \Lambda\tau(a^\dagger\sigma_- + a\sigma_+). \quad (2)$$

This is now block diagonal in the dressed orbital state basis and the overall basis also has a spinor part: $\{[|+\rangle,|-\rangle]\otimes[|\psi_c,n\rangle,|\psi_v^\tau,n+1\rangle]\}$. The cavity and the spin parts $(|+\rangle,|-\rangle)$ are decoupled without an in-plane magnetic field.

We estimate Λ for a simple rectangular cavity of volume $V = l_x l_y l_z$, where the $[011]_{TE}$ mode gives nonzero electric field only along x. We choose $l_x = 0.25\ \mu$m, $l_z = 0.75\ \mu$m and constrain $l_y = [(\omega_-/4\pi c)^2 - l_z^{-2}]^{-1/2} = 0.446\ \mu$m for Λ_- coupling in MoS_2. Note that l_x is allowed to be even smaller for the $[011]_{TE}$ mode which results in stronger cavity coupling. The coupling constants for different TMDC monolayers are shown in Table I for two different transitions: $\Lambda_\pm \propto u\sin(\kappa_y y)\sin(\kappa_z z)[\epsilon_o V(E_g \pm \Delta_{so})]^{-1/2}$. An etched Bragg reflector is a possible cavity candidate. Using Lindblad analysis, we explicitly show in this paper that a cavity quality factor $Q = 10^5$ is required. Roughly, $\Lambda_\pm > \omega_\pm/4Q$ to observe Rabi flops. It should be noted that various high-Q cavities in the optical regime have considerably matured over the years [30,31], with Q reaching 10^9 [32].

The direct product of the photon state and the valance band wave function at initial time $t = 0$ is $\Psi_{\pm,\mathbf{k}}^{\tau,v} = \sum C_n|\psi_v^\tau;\pm;n\rangle$, where $|C_n|^2$ is the probability distribution number of n photons. The wave function at time t is obtained by time evolving with $U = \exp(-iHt)$.

Since the two valleys do not couple with each other one can only consider intravalley optical effects in the present model. For a given valley, in the absence of an external magnetic field, the valence-to-conduction-band (CB) population inversion in the cavity is

$$\mathcal{W}_\pm^\tau(\mathbf{k}) = \sum_n |C_n|^2\left[\vartheta_\pm\cos\left(\frac{\nu_\pm^\tau t}{2}\right) + \varphi_\pm\sin\left(\frac{\nu_\pm^\tau t}{2}\right)\right], \quad (3)$$

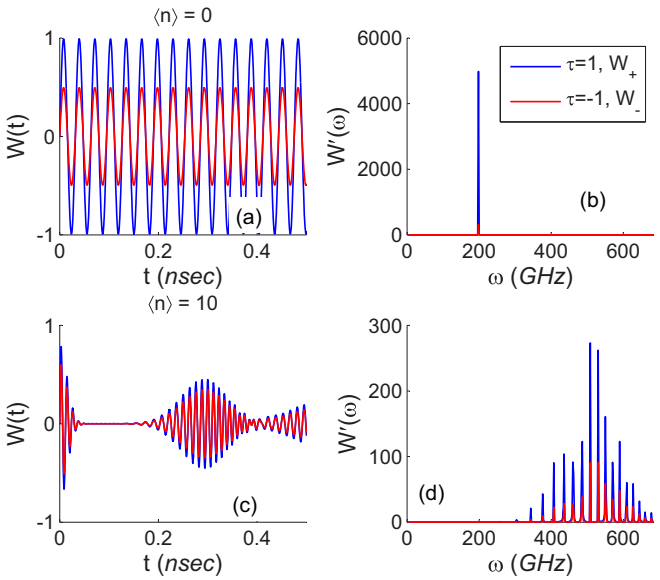

FIG. 2. The spin selection effects of using CPL on the TMDC cavity-QED system as per Fig. 1. Relative spin- or valley-polarized Rabi oscillations shown in (a) for $\tau = \pm 1$ valleys and its corresponding Fourier spectra shown in (b) for $\langle n \rangle = 0$. Here (c) and (d) is the same but for $\langle n \rangle = 10$. For both valleys, the cavity is resonant at $\omega = E_g - \Delta_{so}$ for a coherent state. The CPL intensity $\langle E \rangle = \Lambda$, which shifts the oscillation frequencies higher.

where

$$\vartheta_\pm = \frac{1 + (\mathcal{E}_\pm{}^2 - \mathcal{L}_\pm^2)}{\{[1 + (\mathcal{E}_\pm + \mathcal{L}_\pm)^2][1 + (\mathcal{E}_\pm - \mathcal{L}_\pm)^2]\}^{1/2}},$$

$$\varphi_\pm = \frac{w_\pm(\mathcal{E}_\pm + \mathcal{L}_\pm) + w_\pm^*(\mathcal{E}_\pm - \mathcal{L}_\pm) + f_\pm(\mathcal{E}_\pm{}^2 - \mathcal{L}_\pm^2 - 1)}{\{[1 + (\mathcal{E}_\pm + \mathcal{L}_\pm)^2][1 + (\mathcal{E}_\pm - \mathcal{L}_\pm)^2]\}^{1/2}},$$

$$\mathcal{E}_\pm = (E_g \pm \tau\Delta_{so})/2(\tau k_x' + i k_y'),$$

$$\mathcal{L}_\pm = \sqrt{(E_g \pm \tau\Delta_{so})^2 + 4\left(k_x'^2 + k_y'^2\right)}/2(\tau k_x' + i k_y').$$

Here $\Lambda_n = \Lambda\sqrt{1+n}$, $k'_{x(y)} = u k_{x(y)}$, $\Omega_\pm^\tau = E_g \pm \tau\Delta_{so} - \omega$, $\nu_\pm^\tau = \sqrt{(\Omega_\pm^\tau)^2 + (\tau k_x' + \tau\Lambda_n)^2 + k_y'^2}$, $f_\pm = \Omega_\pm^\tau/\nu_\pm^\tau$, and $w_\pm = (\tau\Lambda_n + \tau k_x' - i k_y')/\nu_\pm^\tau$. The $\pm$ signs represent different spin states. Since these transitions are also $\mathbf{k}$ dependent, the overall inversion probability is obtained after integrating over $\mathbf{k}$, $\mathcal{W}_\pm^\tau = \int \mathcal{W}_\pm^\tau(\mathbf{k}) d\mathbf{k}$.

III. DISCUSSION

A. Valley-selectable photonic spin oscillator

In the absence of B_y, in a monolayer TMDC, only interband transitions between bands of the same spin are allowed. We assume that the single cavity mode is initially in a coherent state, $|C_n|^2 = \exp(-\langle n \rangle)\frac{\langle n \rangle^n}{n!}$ where $\langle n \rangle$ is the average photon number.

For a drive resonant with the gap, $\omega = E_g - \Delta_{so}$, the vacuum Rabi oscillations are shown in Fig. 2(a) along with the corresponding Fourier spectra in Fig. 2(b). For $\langle n \rangle = 0$ there is spontaneous emission and Rabi flipping for the TLS. For the opposite spin states (with gap $E_g + \Delta_{so}$), the maximum Rabi oscillation amplitude ~ 0 since ω is off-resonance with this transition.

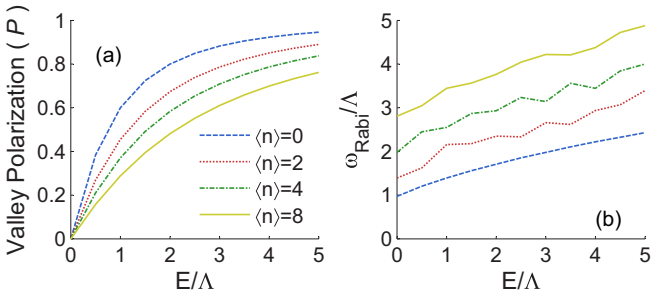

FIG. 3. (a) Valley polarization and (b) peak Rabi frequency shift as a function of CPL intensity and for different photon numbers.

The valley-dependent Rabi oscillations are shown in Fig. 2. These are pure spin oscillations from the cavity coupling. A bias for a particular valley (hence spin) is created by using CPL of a given handedness. We use an additional canonical transformation for introducing CPL, $k_x' \to k_x' + \langle E_x \rangle$ and $k_y' \to k_y' \pm i\langle E_y \rangle$ where $\langle E_x \rangle = \langle E_y \rangle = \langle E \rangle$ and $\langle E \rangle$ is the time-averaged field. Right CPL favors the $\tau = 1$ valley as shown in Fig. 2 since it biases the Hamiltonian by adding a $\langle E_x \rangle \tau\tilde{\sigma}_x + i\langle E_y \rangle\tilde{\sigma}_y$ term.

When $\langle n \rangle > 0$, the Rabi oscillations undergo collapse and revival (CR) which are more rapid, more distinct, and temporally spaced further apart with increasing $\langle n \rangle$. Each term in the summation over n represents Rabi flips weighted by C_n, which are all correlated at $t = 0$. However, at longer times the destructive interference between the weighted terms leads to the collapses and then constructive interference leads to revivals. Figure 2(c) shows that this purely quantum-mechanical CR feature can be individually observed for each valley. This CR happens even in the presence of CPL, but the amplitudes of the CRs are inequivalent for each valley, and they continue indefinitely with each revival being smaller in amplitude and less distinct from the preceding collapse. The Fourier spectra shows a *frequency-comb*-type behavior, where the number of spectral peaks is $\propto \langle n \rangle$. In the present treatment CPL blue-shifts the central Rabi frequency peak, which is discussed in greater detail next.

The valley (spin) polarization in this system can be characterized as follows:

$$\mathcal{P} = \frac{|\mathcal{W}_+^{\tau=1}|_{\max}^2 - |\mathcal{W}_-^{\tau=-1}|_{\max}^2}{|\mathcal{W}_+^{\tau=1}|_{\max}^2 + |\mathcal{W}_-^{\tau=-1}|_{\max}^2}. \quad (4)$$

The degree of valley polarization depends on the CPL's intensity $\langle \mathcal{E} \rangle$ as shown in Fig. 3(a). As $\langle \mathcal{E} \rangle$ is increased, $\mathcal{P}$ tends toward 1, but it also tends to saturate. For a given $\langle \mathcal{E} \rangle$, $\mathcal{P}$ is higher for smaller $\langle n \rangle$. This is because the cavity photons are also vibrating along x which will tend to make the incident light more elliptically polarized as $\langle n \rangle$ is increased. Increasing $\langle \mathcal{E} \rangle$ also shifts the central Rabi frequency peak toward higher frequencies as shown in Fig. 3(b), since CPL increases the effective Λ (see $\nu_\pm^\tau$). The slope $d\omega/d\langle \mathcal{E} \rangle$ is roughly the same for all $\langle n \rangle$ as expected.

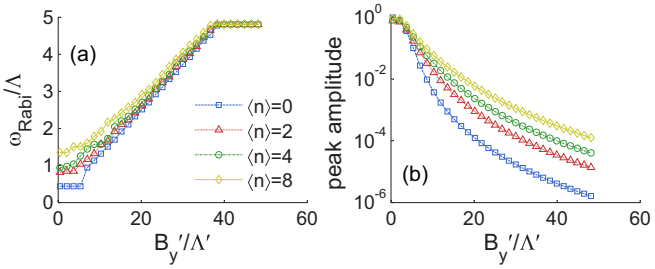

FIG. 4. (a) Normalized peak Rabi frequency as a function of the normalized magnetic field for different $\langle n\rangle$. (b) Corresponding peak oscillation amplitude for the Λ_+ same spin population transfer for $\tau = 1$. Here $\omega = E_g + \Delta_{so}$, $\Lambda' = \hbar\Lambda_+$, and $B_y' = g_\parallel \mu_B B_y$.

A spin-Zeeman field along z does not affect these results; it just adds a phase factor. In experiments it has been shown that the valley degeneracy can be lifted by the valley-Zeeman effect [33,34] where an external magnetic field affects the valley exciton and trion dispersions.

The addition of an in-plane B_y field, however, leads to level detuning and leakages—but again, it does not affect the overall $\mathcal{P}$ for this system for $g_\parallel B_y$ up to 4 T. However, the inclusion of B_y here reveals a technological application of a 2D cavity-QED system.

B. Application as a magnetometer

A monolayer TMDC in an optical cavity can be used for sensitive magnetic field sensing applications. For a 2D material, B_y only affects the spin states and does not lead to the formation of Landau levels. However, now the two orbital TLSs are not decoupled anymore and the dynamics of this system is significantly altered in the presence of B_y. We numerically calculate the population transfer probabilities in the 4×4 dressed state basis.

The magnetic field modifies the zone-center energies to $E_g/2 \pm B_y$ and $-E_g/2 \mp \sqrt{B_y^2 + \Delta_{so}^2}$, which leads to level detuning. This leads to an increase in the Rabi oscillation frequency and a decrease in the oscillation amplitude. The peak Rabi-flop frequencies are shown as a function of a normalized B_y'/Λ for different photon numbers for the drive $\omega = E_g - \Delta_{so}$ in Fig. 4.

At low B_y, ω_{peak} does not change much. And at higher B_y, ω_{peak} saturates. However, the results in the intermediate regime are extremely encouraging. First, the linear scaling of ω_{peak} with B_y, and the invariance of this linear scaling and its slope with B_y/Λ implies that this device can be used as a very sensitive magnetometer.

This is a key result. Usually very strong cavity coupling is desired. Here because of the invariance as a function of B_y/Λ one could get to very small magnetic field sensing limits. This is only possible because of the unique combination of a gapped material with large SO interactions in a 2D geometry—all of which are necessary. The direct gap makes the system optically active and the 2D geometry allows B_y to couple to spin without introducing unwanted Landau levels which then subsequently couples the CB orbitals.

In theory these effects can be reproduced if one just added a $B_y\sigma_y$ term to the Jaynes-Cummings Hamiltonian. But physically one cannot have an electric dipole coupling and a magnetic field coupling in the same matrix element for an orbital two-level system. We also argue that this would be robust even with cavity imperfections and spin dephasing and relaxation as one is not concerned with the decay of the signal, but just with the main Fourier peak. Experimentally this amounts to spectrally decomposing the time-dependent photoluminescence signal.

C. Persistent intervalley conduction-band oscillations

In the presence of B_y, either direct or indirect transitions between all four states in a valley are allowed. However, some rather peculiar features stand out for the CB $\psi_{c,-} \leftrightarrow \psi_{c,+}$ transitions. These results were obtained by exact numerics by unitarily time evolving the system using $U = \exp(-iHt)$, and projecting the dressed $\psi_{c,\pm}$ CB eigenstates of H_o'.

The Rabi flops for these transitions are shown in Fig. 6. At very small but finite B_y, the vacuum Rabi flops reach 1. As the magnetic field strength increases, the amplitude decreases, but the Rabi frequency does not shift. But again, if $B_y = 0$, this Rabi flopping would vanish.

This behavior can be explained analytically. Note that in general $[H_0, H_b] \neq 0$; however, in order to gain better intuition one can approximate $U \approx e^{-iHt}e^{-iH_bt}$, which is valid for small B_y. Then the CB population inversion is

$$\langle \Psi_-^c|U|\Psi_+^c\rangle \sim \cos(B_y t)(\mathcal{W}'_+ - \mathcal{W}'_-) + i\sin(B_y t)(\mathcal{C}_+\mathcal{W}'_+ - \mathcal{C}_-\mathcal{W}'_-), \quad (5)$$

where $\mathcal{C}_\pm = (\sqrt{B_y^2 + \Delta_{so}^2} \pm \tau\Delta_{so})/B_y$ and $\mathcal{W}'_\pm = \sum |C_n|^2[\cos(\frac{\nu_\pm t}{2}) + \frac{\Omega_\pm}{\nu_\pm}\sin(\frac{\nu_\pm t}{2})]$. Equation (5) approaches 1 in the limit of a vanishing B_y.

The peculiar Rabi flopping in Fig. 6(a) can therefore be explained as follows. In the absence of a magnetic field, the CB $c_\pm$ states are degenerate but are completely decoupled from each other in the present $\mathbf{k}\cdot\mathbf{p}$ model. An infinitesimally small B_y lifts this degeneracy and couples the two CB states allowing $\Psi_-^c \leftrightarrow \Psi_+^c$ transitions. However, now since the two levels are still nearly degenerate for a small B_y, there is an almost perfect overlap of the wave functions. As a result the Rabi flops reach 1 for infinitesimally small B_y's. Equation (5) reproduces this behavior in the limit of small B_y. As the magnetic field strength increases, the amplitude decreases, but the Rabi frequency does not shift.

We also examine the photon number dependence of this behavior. In Figs. 6(a) and 6(b) the dependence for $\langle n\rangle = 0$ and $\langle n\rangle = 10$ is respectively shown. For $\langle n\rangle = 10$, the collapseand revival type behavior is seen for these conduction-band states as expected. Like the $\langle n\rangle$ case, no notable distinction can be drawn between the $\langle n\rangle = 10$ $g_{||}B_y = 0.1T$ and $0.01T$ cases because of the nearly degenerate CB states.

This behavior is characterized more carefully in Fig. 5 where the maxima of the Rabi oscillations between *opposite* spin conduction-band states is shown as a function of the magnetic field and different photon numbers. The Rabi oscillation amplitudes and frequencies remain relatively unaffected for smaller magnetic fields.

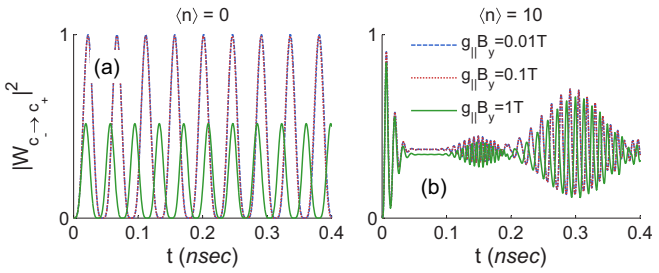

FIG. 5. Population transfer between *opposite* spin conduction-band states: $\psi_{c,-} \leftrightarrow \psi_{c,+}$ shown for different photon numbers and magnetic fields for $\omega = E_g - \Delta_{so}$ and $\tau = 1$.

The energy gap between the spin-split conduction-band states is $2\mu_B g_{||} B_y$. It should be noted that in actual TMDC monolayers, the CB states are also nondegenerate and spin split, although the spin splitting is far smaller than that of the valence band [17,35,36]. While this CB splitting does not affect the other results, the CB population transfer amplitudes would be less than what is shown in Fig. 6. Overall, this is an important effect to take into account when considering quantum information processing applications since the Rabi oscillations would be insensitive to small magnetic field fluctuations such as from nuclear spins.

D. Cavity imperfections and finite exciton lifetimes

Finally we consider system imperfections such as cavity losses and finite exciton lifetimes which will lead to decoherence. In TMDCs free-electron–hole pairs in different valleys respond to CPL of different handedness. However, in the case of excitons—bound-electron–hole pairs. The electrons in one valley interact with the holes in the other valley resulting in both bright and dark excitons. These interactions result in the excitonic dispersion having a longitudinal (L) and a transverse (T) split as a function of its center-of-mass momentum $\mathcal{K}$. The L and T levels respond to two orthogonal linearly polarized modes of light. This splitting between exciton states with opposite angular momentum can also be explained in terms of the Berry curvature using a gapped two-band Dirac model [37]. Other variants of the massive Dirac model have also

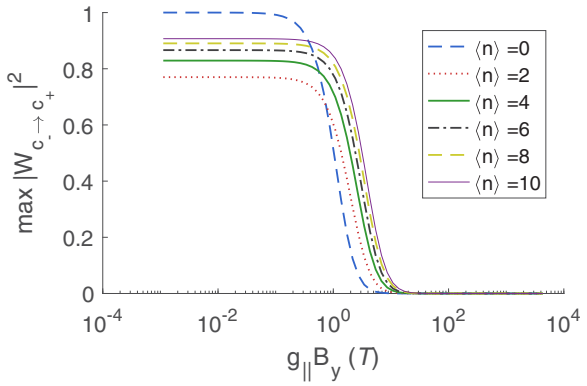

FIG. 6. Maxima of the Rabi oscillations between *opposite* spin conduction-band states as a function of the magnetic field and different photon numbers. Here $\omega = E_g - \Delta_{so}$ and $\tau = 1$.

been used to explain the properties of excitons in TMDCs [38,39]. However, the excitonic band-structure calculations differ. Some studies show that the exciton bands split into a lower parabolic band and an upper parabolic and nonanalytic branch [40].

In general, bright and dark excitonic transitions at $\mathcal{K} = 0$ and $\mathcal{K} = K$ are allowed. The massive Dirac model captures many of the useful features of the $\mathcal{K} = 0$ excitons which mainly contribute to the optical properties. In this paper we examine the cavity QED of excitons within the framework of a simple two-band massive Dirac model [37–39] about $\mathcal{K} = 0$ and for a $1s$-level exciton gap ω_x. Following the procedure to derive Eq. (2), we arrive at

$$H' = u\vec{\mathcal{K}} \cdot \vec{\sigma} + \frac{\omega_x}{2}\sigma_z + \frac{\omega}{2}a^\dagger a + \Lambda(a^\dagger\sigma_- + a\sigma_+). \quad (6)$$

Excitons have finite lifetimes which along with the cavity imperfections places limitations on the number of Rabi flops that can be observed before they decohere. The experimentally measured radiative lifetime of excitons in monolayer MoS_2 is about 820 ps [41] which is very similar to other monolayer TMDCs [42]. Here we assume a relaxation time of $T_1 = 800$ ps and also consider the cavity imperfections via its quality factor. The various dissipative processes will result in mixed states and hence solutions can be sought in terms of the density operator. Here we model the decoherence effects using the Lindblad equations

$$\dot{\rho}' = -\frac{i}{\hbar}[\rho', H] + \Gamma_Q \mathscr{L}(a, \rho') + \Gamma_e \mathscr{L}(\sigma, \rho'), \quad (7)$$

where $\mathscr{L}(a,\rho) = a^\dagger a\rho + \rho a^\dagger a - 2a\rho a^\dagger$ and $\mathscr{L}(\sigma,\rho) = \sigma_+\sigma_-\rho + \rho\sigma_-\sigma_+ - 2\sigma_-\rho\sigma_+$, $\Gamma_Q = \omega_\pm/Q$, and Γ_e is the exciton relaxation rate. The Lindbald equation can be solved in the superoperator form:

$$\vec{\rho}'(t) = \exp(-\mathcal{S}t)\vec{\rho}'(0), \quad (8)$$

where $\vec{\rho}$ is a vector and for exciton relaxation, e.g., the superoperator: $\mathcal{S} = -iH \otimes I + iI \otimes H + \sigma_- \otimes \sigma_+ - \frac{1}{2}(\sigma_+\sigma_- \otimes I + I \otimes \sigma_+\sigma_-)$. We assume that at $t = 0$, the TMDC's pseudospin and the single cavity mode are unentangled pure states, i.e., $\rho(0) = \rho_s(0) \otimes \rho_c(0)$, where the initial density operator for the pseudospin is $\rho_s(0) = |\psi_v^\tau\rangle\langle\psi_v^\tau|$ and for the cavity field is $\rho_c(0) = \sum_n |C_n|^2 |n\rangle\langle n|$. We then solve Eq. (8) and take a partial trace over the cavity field $\rho' = \mathrm{Tr}_c[\rho_c\rho_s]$.

The density matrix can be decomposed into its constituent Bloch vector components $\rho' = I + \sum \eta_j \sigma_j$ where $j \in \{x, y, z\}$. In Fig. 7(a), the expectation values $\langle\eta_j\rangle = \mathrm{Tr}(\sigma_j\rho)$ are shown as a function of time for a perfect cavity, with $\langle n\rangle = 0$ and $T_1 = 800$ ps. Note that $\langle\eta_y\rangle$ and $\langle\eta_z\rangle$ are $\pi/2$ out of phase as expected and are the two nonzero values as the electric field is oscillating about x.

For a perfect cavity, numerous Rabi flops can be observed as shown in Fig. 7(a) due to the strong cavity coupling and long exciton life times. The greater limiting factor for cavity QED with monolayer TMDC would be the cavity imperfections as shown in Fig. 7(b). The exciton T_1 lifetime is also included here. For the Λ considered here, No Rabi oscillations will be seen for $Q = 10^3$ while they are significantly long-lived for

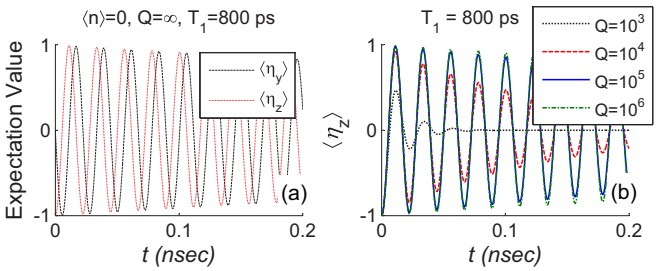

FIG. 7. (a) Expectation value of the Bloch vector components $\langle\eta_y\rangle$ and $\langle\eta_z\rangle$ as a function of time for a perfect cavity, $Q=\infty$, and an excitonic relaxation time of $T_1 = 800$ ps. (b) Expectation value of $\langle\eta_z(t)\rangle$ for imperfect cavities with varying Q's and an excitonic relaxation time of $T_1 = 800$ ps.

$Q = 10^5$. Further improvements for $Q = 10^6$ are quite small where the exciton lifetime is now the limiting factor.

IV. SUMMARY

In summary the photonic cavity's strong coupling to lattice pseudospin leads to various interesting effects for an inversion asymmetric monolayer TMDC. This system can act as an on-chip coherent light source. The Dirac-type Hamiltonian for a 2D gapped semiconductor with a large SO interaction facilitates pure Jaynes-Cummings coupling for a single-mode electric field. This gives rise to valley- and spin-dependent optical properties which can be controlled in a 2D architecture by using an additional CPL field. With CPL and strong coupling effects *spontaneous* vacuum spin oscillations can occur. Valley-selective collapse and revival of Rabi oscillations occur for higher photon number coherent states. These effects would be easily observable for $Q \sim 10^5$.

The presence of an external in-plane magnetic field leads to additional interesting effects. The TMDC cavity-QED device can be used for sensitive magnetic field sensing applications, which is possible because of the combination of a gapped 2D material with large SO interactions and a 2D optical cavity. As a consequence of B_y, Rabi oscillations between nearly degenerate opposite-spin CB states become feasible in direct gapped monolayer TMDC. These oscillations are also robust against small magnetic field fluctuations which could be useful for quantum information applications.

ACKNOWLEDGMENTS

This work was supported by the NSF 2-DARE, EFRI-1433395 and by FAME, one of six centers of STARnet, a Semiconductor Research Corporation program sponsored by MARCO and DARPA.

[1] D. Leibfried, R. Blatt, C. Monroe, and D. Wineland, Rev. Mod. Phys. **75**, 281 (2003).
[2] R. J. Thompson, G. Rempe, and H. J. Kimble, Phys. Rev. Lett. **68**, 1132 (1992).
[3] J. M. Raimond, M. Brune, and S. Haroche, Rev. Mod. Phys. **73**, 565 (2001).
[4] K. Hennessy, A. Badolato, M. Winger, D. Gerace, M. Atatüre, S. Gulde, S. Fält, E. L. Hu, and A. Imamoğlu, Nature (London) **445**, 896 (2007).
[5] A. A. Kovalev, A. De, and K. Shtengel, Phys. Rev. Lett. **112**, 106402 (2014).
[6] Ö. O. Soykal, R. Ruskov, and C. Tahan, Phys. Rev. Lett. **107**, 235502 (2011).
[7] M. H. Devoret, D. Esteve, J. M. Martinis, and C. Urbina, Phys. Scr. **1989**, 118 (1989).
[8] R. J. Schoelkopf and S. M. Girvin, Nature (London) **451**, 664 (2008).
[9] J. M. Martinis, Quant. Inf. Proc. **8**, 81 (2009).
[10] A. Blais, R.-S. Huang, A. Wallraff, S. M. Girvin, and R. J. Schoelkopf, Phys. Rev. A **69**, 062320 (2004).
[11] L.-M. Duan and H. J. Kimble, Phys. Rev. Lett. **92**, 127902 (2004).
[12] A. M. Jones, H. Yu, N. J. Ghimire, S. Wu, G. Aivazian, J. S. Ross, B. Zhao, J. Yan, D. G. Mandrus, D. Xiao *et al.*, Nat. Nanotechnol. **8**, 634 (2013).
[13] X. Xu, W. Yao, D. Xiao, and T. F. Heinz, Nat. Phys. **10**, 343 (2014).
[14] A. M. Jones, H. Yu, J. S. Ross, P. Klement, N. J. Ghimire, J. Yan, D. G. Mandrus, W. Yao, and X. Xu, Nat. Phys. **10**, 130 (2014).
[15] K. He, N. Kumar, L. Zhao, Z. Wang, K. F. Mak, H. Zhao, and J. Shan, Phys. Rev. Lett. **113**, 026803 (2014).
[16] A. Chernikov, T. C. Berkelbach, H. M. Hill, A. Rigosi, Y. Li, O. B. Aslan, D. R. Reichman, M. S. Hybertsen, and T. F. Heinz, Phys. Rev. Lett. **113**, 076802 (2014).
[17] A. Kormányos, V. Zólyomi, N. D. Drummond, and G. Burkard, Phys. Rev. X **4**, 011034 (2014).
[18] Z. Gong, G.-B. Liu, H. Yu, D. Xiao, X. Cui, X. Xu, and W. Yao, Nat. Commun. **4**, 2053 (2013).
[19] L. Britnell, R. Ribeiro, A. Eckmann, R. Jalil, B. Belle, A. Mishchenko, Y.-J. Kim, R. Gorbachev, T. Georgiou, S. Morozov *et al.*, Science **340**, 1311 (2013).
[20] X. Gan, K. F. Mak, Y. Gao, Y. You, F. Hatami, J. Hone, T. F. Heinz, and D. Englund, Nano Lett. **12**, 5626 (2012).
[21] F. H. Koppens, D. E. Chang, and F. J. García de Abajo, Nano Lett. **11**, 3370 (2011).
[22] V. Menon, Nat. Mater. **14**, 370 (2015).
[23] Y. Ye, Z. J. Wong, X. Lu, H. Zhu, X. Chen, Y. Wang, and X. Zhang, Nat. Photonics **9**, 733 (2015).
[24] S. Schwarz, S. Dufferwiel, P. Walker, F. Withers, A. Trichet, M. Sich, F. Li, E. Chekhovich, D. Borisenko, N. N. Kolesnikov *et al.*, Nano Lett. **14**, 7003 (2014).
[25] S. Wu, S. Buckley, J. R. Schaibley, L. Feng, J. Yan, D. G. Mandrus, F. Hatami, W. Yao, J. Vučković, A. Majumdar *et al.*, Nature (London) **520**, 69 (2015).
[26] D. Xiao, G.-B. Liu, W. Feng, X. Xu, and W. Yao, Phys. Rev. Lett. **108**, 196802 (2012).
[27] I. J. Hodgkinson, Q. h. Wu, M. Arnold, M. W. McCall, and A. Lakhtakia, Opt. Commun. **210**, 201 (2002).

[28] A. A. Maksimov, I. I. Tartakovskii, E. V. Filatov, S. V. Lobanov, N. A. Gippius, S. G. Tikhodeev, C. Schneider, M. Kamp, S. Maier, S. Höfling *et al.*, Phys. Rev. B **89**, 045316 (2014).
[29] K. Konishi, M. Nomura, N. Kumagai, S. Iwamoto, Y. Arakawa, and M. Kuwata-Gonokami, Phys. Rev. Lett. **106**, 057402 (2011).
[30] K. J. Vahala, Nature (London) **424**, 839 (2003).
[31] G. Khitrova, H. Gibbs, M. Kira, S. Koch, and A. Scherer, Nat. Phys. **2**, 81 (2006).
[32] H. Lee, T. Chen, J. Li, K. Y. Yang, S. Jeon, O. Painter, and K. J. Vahala, Nat. Photonics **6**, 369 (2012).
[33] G. Aivazian, Z. Gong, A. M. Jones, R.-L. Chu, J. Yan, D. G. Mandrus, C. Zhang, D. Cobden, W. Yao, and X. Xu, Nat. Phys. **11**, 148 (2015).
[34] A. Srivastava, M. Sidler, A. V. Allain, D. S. Lembke, A. Kis, and A. Imamoğlu, Nat. Phys. **11**, 141 (2015).
[35] N. Zibouche, A. Kuc, J. Musfeldt, and T. Heine, Ann. Phys. (Berlin) **526**, 395 (2014).
[36] A. Kormányos, G. Burkard, M. Gmitra, J. Fabian, V. Zólyomi, N. D. Drummond, and V. Fal'ko, 2D Mater. **2**, 022001 (2015).
[37] J. Zhou, W.-Y. Shan, W. Yao, and D. Xiao, Phys. Rev. Lett. **115**, 166803 (2015).
[38] F. Wu, F. Qu, and A. H. MacDonald, Phys. Rev. B **91**, 075310 (2015).
[39] H. Yu, G.-B. Liu, P. Gong, X. Xu, and W. Yao, Nat. Commun. **5**, 3876 (2014).
[40] D. Y. Qiu, T. Cao, and S. G. Louie, Phys. Rev. Lett. **115**, 176801 (2015).
[41] H. Shi, R. Yan, S. Bertolazzi, J. Brivio, B. Gao, A. Kis, D. Jena, H. G. Xing, and L. Huang, ACS Nano **7**, 1072 (2013).
[42] M. Palummo, M. Bernardi, and J. C. Grossman, Nano Lett. **15**, 2794 (2015).